Available online at www.sciencedirect.com
SCIENCE DIRECT®
Geomorphology 57 (2004) 151–167
GEOMORPHOLOGY
www.elsevier.com/locate/geomorph

Combining field and modelling techniques to assess rockfall dynamics on a protection forest hillslope in the European Alps

Luuk K.A. Dorren[a,*], Bernhard Maier[b], Uif S. Putters[a], Arie C. Seijmonsbergen[a]

[a] *Centre for Geo-ecological Research (ICG), Institute for Biodiversity and Ecosystem Dynamics-Physical Geography, Universiteit van Amsterdam, Nieuwe Achtergracht 166, 1018 WV Amsterdam, The Netherlands*
[b] *Stand Montafon-Forstfonds, Montafonerstraße 21, A-6780 Schruns, Austria*

Received 19 June 2002; received in revised form 7 February 2003; accepted 9 February 2003

Abstract

Adequate management of a mountain forest that protects downslope areas against impacts of rockfall requires insight into the dynamics of the hillslope environment. Therefore, we applied a combined approach, using field and modelling techniques, to assess the determining factors for rockfall source areas, rockfall tracks and rockfall runout zones on a forested slope in mountainous terrain. The first objective of this study was to understand why rockfall occurs in the study area. The second objective was to translate the knowledge obtained in the field into a model that simulates rockfall dynamics on a forested slope realistically. The third objective was to assess which hillslope characteristics primarily determine the distribution of active rockfall tracks. To achieve these objectives, we made a geomorphological map of the whole study area, and we measured the major discontinuity planes in the bedrock that are exposed in the rockfall source areas. Furthermore, a test site for simulation modelling within the larger study area was defined in which both a forest and a hillslope inventory were carried out. The available data and our developed rockfall simulation model allowed us to assess the slope characteristics that mainly determine the distribution of areas affected by rockfall. We found that in decreasing order of importance, both standing and felled trees, the surface roughness and rockfall resistant shrubs primarily determine the distribution of rockfall-affected areas. Simulation tests without a forest cover produced similar rockfall runout zones as fossil rockfall events identified in the field. We believe that the combined field and modelling approach is a prerequisite for understanding how forests can protect against rockfall.

Keywords: Rockfall; European Alps; Hillslope

1. Introduction

Many mountain forests protect against rockfall, which might pose serious risks to local inhabitants, their houses as well as infrastructure (Jahn, 1988; Motta and Haudemand, 2000). However, it is often unknown whether the protective function of a forest covering an active rockfall slope is effective enough. The protective function of the forests could decrease as a result of the continuous disturbance caused by impacts of falling rocks. Therefore, it is difficult to predict whether the protective function of a forest covering an active rockfall slope remains effective

* Corresponding author. Tel.: +31-20-5257420; fax: +31-20-5257431.
E-mail address: l.dorren@science.uva.nl (L.K.A. Dorren).

0169-555X/$ - see front matter © 2003 Elsevier B.V. All rights reserved.
doi:10.1016/S0169-555X(03)00100-4

through time. This depends on the forest dynamics, which are strongly affected by rockfall, since the distribution as well as the frequency and magnitude of rockfall events determine the development of a forest covering the accumulation area of an active rockfall source area. At the same time, the distribution of trees on a forested rockfall slope affects the distribution, frequency and magnitude of rockfall events (Jahn, 1988). In other words, there is an interaction between rockfall and forest cover. Therefore, dynamics of a forested rockfall slope could only be studied by focusing on both forest characteristics and rockfall dynamics.

Until now, rockfall dynamics have mainly been investigated by geotechnical measurements in rockfall source areas (Wieczorek et al., 2000; Zvelebil and Moser, 2001), talus slope inventories (Statham and Francis, 1986; Evans and Hungr, 1993; Bull et al., 1994; Wieczorek and Jäger, 1996; Jomelli and Francou, 2000; Hétu and Gray, 2000), experimental tests in laboratories or on nonforested hillslopes (Kirkby and Statham, 1975; Chau et al., 1998; Okura et al., 2000a) and simulation modelling studies (Statham, 1976; Bozzolo and Pamini, 1986; Azzoni et al., 1995; Budetta and Santo, 1994; Okura et al., 2000b). Little work has been done on the interaction between rockfall and protection forests. Within this study, we applied a combined approach, using both field and modelling techniques, to assess the determining factors for rockfall source areas, their tracks and runout zones on a forested slope in mountainous terrain where rockfall is highly active. As a basis for this study, we formulated the following research questions:

1. Why do the rockfall source areas occur in the study area?
2. Could the knowledge obtained in the field be translated into a model that simulates realistic rockfall dynamics on a forested slope?
3. Which environmental characteristics primarily determine the distribution of areas affected by active rockfall?

2. Study area

The area investigated in this study was the "Außerbacher" forest, which is located near the village of Gaschurn in the Montafon region in the western part of Austria, between 47°8′ and 46°50′ latitude and 9°41′ and 10°9′ longitude. The altitude of the study area ranges from 930 m above sea level in the valley floor up to 1500 m above sea level. The forest in the area covers a south–southwest exposed slope, which may be divided in a source area, which has a mean slope gradient of 60° and an accumulation area, which has a mean slope gradient of 30°. The underlying geology, which is metamorphic bedrock, consists of amphibolites, mica schists and white/grayish ortho-(granite bearing) gneisses. The resistant amphibolites and gneisses were subject to strong glacial abrasion. Therefore, steep cliff faces developed. These faces are currently active rockfall source areas. In between the steep cliff faces, three major denudation niches are present, which are connected with distinct open tracks in the forest (Fig. 1).

The forest covering the study area is a typical mixed mountain forest, which is found on many vegetated talus/debris cones in the montane zone in the European Alps. The dominating species in the study area are primarily Norway spruce (*Picea abies*) and, to a lesser extent, sycamore (*Acer pseudoplatanus*), beech (*Fagus silvatica*) and hazel (*Corylus avellana*). The lower part of the study area is well accessible by two forest roads, which have been constructed for forest management practices (see Fig. 1).

3. Procedures

Fieldwork started with a reconnaissance and detailed geomorphological mapping on the basis of the mapping system described by De Graaff et al. (1987) and Seijmonsbergen (1992), after identifying the main landform units in the study area by interpreting false colour stereographic aerial photographs. Printed colour-infrared (CIR) orthophotos from 1996 with a resolution of 0.25 × 0.25 m, produced by the National Austrian Mapping Agency (BEV), served as a basis for mapping. The slope gradient and the exposition of the slope face as well as the dip and dip direction of the bedding planes and the most prominent joint sets were measured at 33 different locations in the rockfall source areas. These measurements were plotted in an equal area projection (Hoek and Bray, 1981) to carry out a Markland test (Markland, 1972; Hocking, 1976).

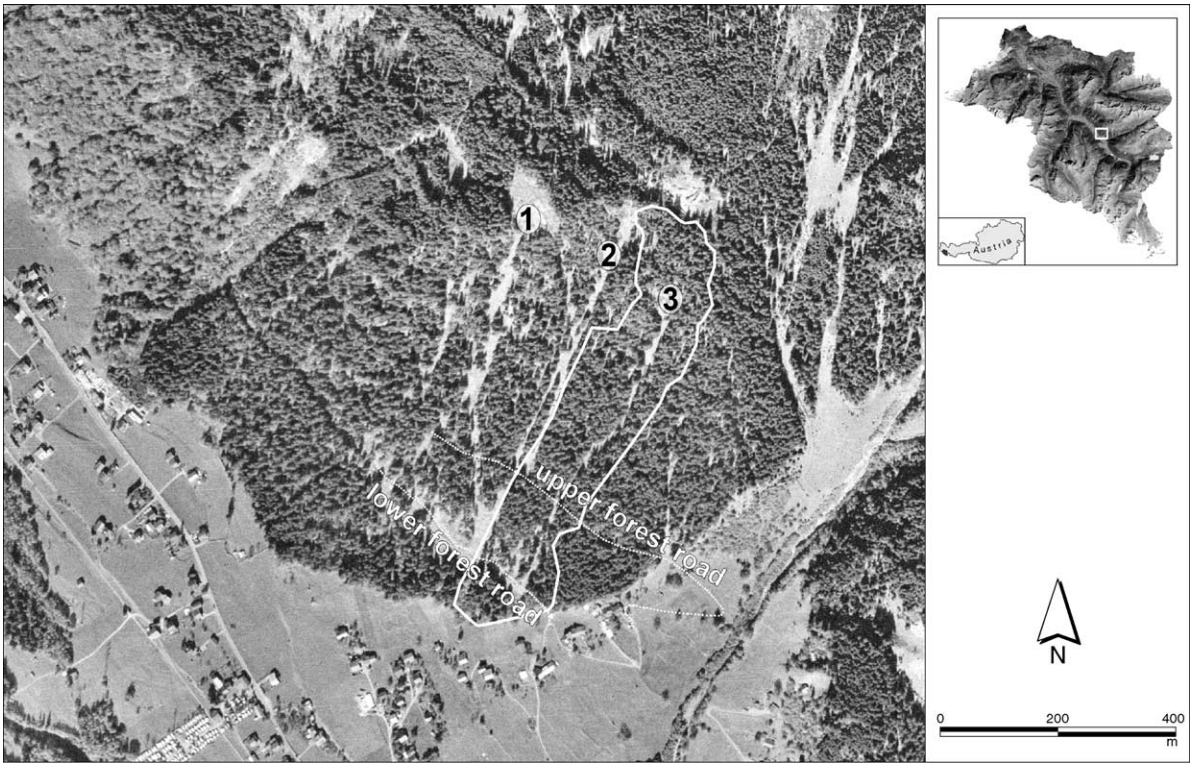

Fig. 1. Orthorectified pan-chromatic aerial photograph from 1987 showing the study area. The white outline demarcates the test site used for simulation modelling within this study. The numbers indicate the three denudation niches and the associated transport channels.

This test was done to identify potential sliding surfaces resulting from discontinuities in the bedrock in relation to the orientation of the local topography.

In addition, we carried out a field inventory to obtain a map of the spatial distribution of different hillslope characteristics that potentially affect rockfall tracks. Polygons representing terrain units with similar properties were mapped. These polygons covered an area varying from 10 to 7000 m^2, depending on the homogeneity of the terrain. For all these polygons, we estimated or measured the following parameters:

- The mean slope gradient (measured with an Abney level).
- The percentage of the surface area covered by bedrock (estimated).
- The granular composition of the material covering the surface, estimated for the top 25 cm. Percentages of contents were estimated for the following fractional classes: <5 cm, 5–20 cm and >20 cm.
- The surface roughness, classified for three transects with a length of 1, 5 and 20 m that were representative for the polygon. For all the three transects, the surface roughness was estimated as type a, b or c on the basis of Fig. 2. This resulted in three roughness values for each polygon.
- The number of barriers created by felled trees. For this, the number of felled trees, lying diagonally or perpendicular to the slope direction over a straight,

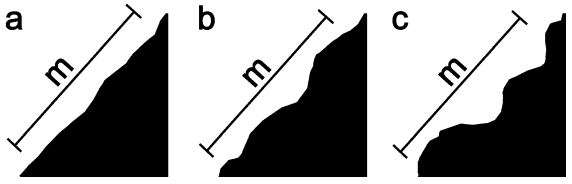

Fig. 2. Surface roughness over a transect length *m* expressed as type a, b, or c.

downslope line of 10 m that was representative for the polygon, was counted.
- The percentage of surface area covered with rockfall resistant shrubs with a height up to 5 m, such as *C. avellana*, was estimated.

Furthermore, we carried out a detailed forest inventory using the *Winkelzählprobe* (Bitterlich, 1948), which is also known as prism plot sampling or probability proportional to size sampling. Within this method, the probability of a tree being selected within a sampling plot is proportional to the basal area of a tree (Shiver and Borders, 1995). For this inventory, we used a grid with cells of 30 × 50 m. This grid almost completely covered the forested part of the test site that was used for the simulation modelling study. It is assumed that data obtained in the sampled areas in the centres of the grid cells are valid for the whole grid cell, which is justified if the *Winkelzählprobe* is used and if data values are expressed per hectare (Shiver and Borders, 1995). The inventory provided standard forest parameters such as the number of trees per hectare, the diameter at breast height (DBH), the basal area and the height of the trees, and also the number of scars on tree stems caused by heavy impacts of falling rocks and the height of these damages on the tree stems.

4. Fieldwork results

4.1. The source area

The slope gradient within the source area varies between 50° and 90°. The mean values of all the slope gradients and expositions as well as the dip and dip direction measurements of the bedding planes and the most prominent joint sets are given in Table 1. The great circles of the planes defined by the mean values given in Table 1 are shown in Fig. 3. The interior dashed circle in Fig. 3 represents the friction angle along discontinuities representative for the study area. The friction angle value of 37° was calculated using the uniaxial compressive strength (see Carson and Kirkby, 1972), which was obtained from a uniaxial compression test applied on three amphibolite samples and on one gneiss sample, in combination with the *Hoek–Brown* criterion (Hoek and Brown, 1997).

Table 1
Geological dip and dip direction measurements of the most important measured planes in the rockfall source area

Plane type	Dip (*slope gradient)	Dip direction (**exposition)
Slope face	*72 ± 14°	**187 ± 30°
Bedding planes	31 ± 12°	000 ± 18°
J1	62 ± 16°	118 ± 24°
J2	58 ± 18°	139 ± 21°

The point of intersection of the two circles for joint set 1 (J1) and joint set 2 (J2), which lies between the friction angle circle and the great circle of the slope face, indicates that these two joint planes create potential wedge failures. Especially in combination with the bedding plane that dips in opposing direction, which creates the 'roof' of potential falling rocks, wedge-shaped blocks are easily produced (Fig. 3). As shown in Table 1, the dip and dip direction values of the two major joint sets and the slope face vary considerably. This results in planar sliding at some locations because the dip and dip direction of the slope and the major joints are identical. We observed in the field that the orientation of both joint sets (J1 and J2) and the orientation of the bedding planes resulted in rocks breaking out at the bottom parts of the steep cliff face. This leads to undercutting of the slope face and subsequent migration of rockfall activity upslope. Fortunately, the joint spacing is generally small and therefore mainly small rocks are produced (largest rock diameter between 0.25 and 0.5 m).

Another factor, which also contributes to rockfall activity in the study area, is the presence of large tensional fissures in the area above the steep cliff face (Fig. 4). These fissures indicate large-scale rock creep. Parallel tensional rebound of the valley slope after glaciation during Late Glacial and Early Holocene conditions was probably the main cause of this. The effect, however, is increased by the presence of mica schist layers underneath the amphibolite and gneiss bedrock layers. The mica schist layers act as weak zones, which cause additional bulging forward and toppling of the creeping bedrock into the valley. As a consequence, the steep cliff face maintains its steepness despite active mass wasting and therefore facilitates slope failures and resulting mass wasting.

Local inhabitants informed us that rockfall generally occurs in spring and after heavy rain, which was

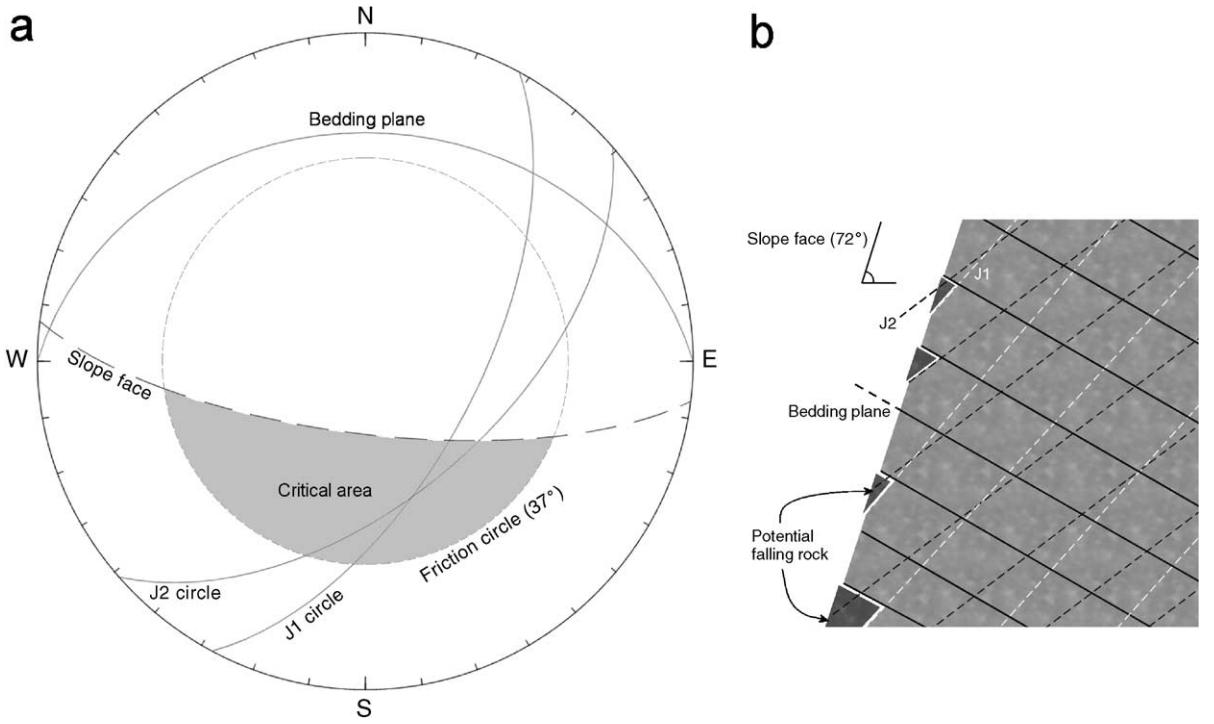

Fig. 3. (a) The lower hemisphere projection of an equal area net showing the great circles of the slope face, the bedding planes and the two most prominent joint sets (J1 and J2). (b) Two-dimensional visualisation of the effect of the intersection of the bedding planes and the joint sets in the rockfall source areas in the study area.

also observed during fieldwork. Unfortunately, the inhabitants were not able to tell which source areas particularly produce falling rocks. The transport channels visible in Fig. 1 suggest that the main rockfall activity occurs within the denudation niches upslope of the transport channels. We observed, however, that the production of potential falling rocks in the study area was not merely concentrated within the niches, but all the steep cliff faces throughout the area acted as rockfall source area. After we completed the geomorphological map, it was interesting to observe that the largest tensional fissures are aligned with the longitudinal direction of the denudation niches. This suggests that the weaker zones that are responsible for the development of the denudation niches have been predetermined by tensional fissuring.

4.2. The accumulation area

The accumulation area is a steep talus cone with a mean slope gradient of 38–40°. Distinct patterns of recent accumulation, indicated by fresh scree, were mainly found in depressions between the largest talus cones and upslope of felled trees, which were positioned diagonally on the slope to act as barriers. The size of the recent accumulated rocks, mainly consisting of amphibolites and some gneisses, generally varied between 0.2 and 0.5 m (diameter of largest rock axis). Smaller rocks and fine material were only found in the transport channels. Other than the areas with recent accumulation, a rather uniform distribution of rocks was found throughout the accumulation area, both with respect to size and inferred deposition period, which was assessed on the basis of moss cover and vegetation cover. Nevertheless, occasional groups of huge rocks (>2 m^3) and lobe-like accumulation forms consisting of nonsorted material were found. All this accumulated material was covered with moss and vegetation. These deposits indicate that both debris flows and rock avalanches do occur. We assume that the main sediment contributions to the

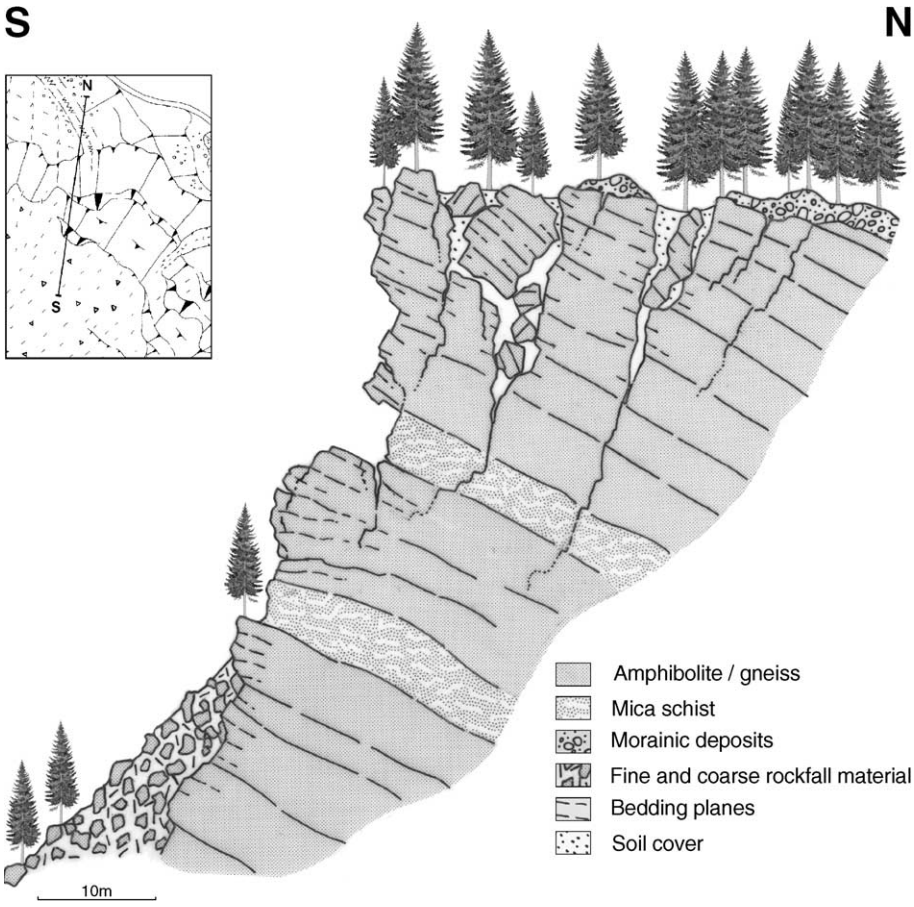

Fig. 4. Cross section showing internal rock deformation due to active large-scale tensional fissuring in the area above the steep cliff faces. The inset shows a part of the geomorphological map of the source area and the location of the cross section.

initial build up of the talus cone after deglaciation were delivered by rock avalanches and debris flows in a non- or scarcely vegetated environment.

The forest inventory was limited to an area that covered the main part of the test site that was used for simulation modelling. The composition of the forest in the test site is shown in Table 2. Although sycamores occur less frequently than Norway spruces, they are more resistant against rock impacts because they have a very good wound healing capacity. However, the number of sycamores in the area remains relatively low because Norway spruce is the dominant tree species.

A large proportion of the trees in the test site are in an ageing or even a breakdown phase, which means that most frequently quite large trees were found, but they were often old and heavily wounded by rock impacts, especially the trees in the upper part of the accumulation area. Bark and stem damage may lead to heart rot, which reduces the individual tree stability. As expected, the number of heavily damaged trees is the largest close to the rockfall source areas, and, generally, this number decreases downslope.

In relation to the ageing and breakdown phase of the forest in the test site, the lack of regeneration, indicated by the absence of seedlings, is problematic for the future protective function of the forest. This is mainly the result of hunting management. For quite a long period, hunters used the forest in the study area as a winter-feeding station for ungulates, which increased the browsing pressure considerably.

Table 2
Forest composition in the study area

Tree name	Species	Coverage in forest (%)			
Norway spruce	*Picea abies*	96			
Sycamore	*Acer pseudoplatanus*	3			
Beech	*Fagus silvatica*	<1			
Hazel	*Corylus avellana*	<1			
General information	Mean	Std. dev.	Minimum	Maximum	
Number of trees/hectare	201	137	0	660	
DBH (cm)	54	18	20	139	

Several studies carried out in forests in the European Alps have shown that ungulate browsing decreases the regeneration of forests (Ammer, 1996; Motta, 1996). In our study area, ungulate browsing has resulted in a situation where regeneration is completely lacking.

5. GIS model development

5.1. Digital elevation model

As observed in the field, the topography determines the occurrence, the direction as well as the velocity of a falling rock. Therefore, a digital elevation model (DEM) is the most relevant dataset for simulating rockfall. We derived a DEM with a support of 2.5 × 2.5 m from a Triangular Irregular Network (TIN), which was produced from contour lines with an equidistance of 5 m using the TOPOGRID module in ArcInfo 7.0 (ESRI, 2003). These contour lines were created on the basis of a combined dataset consisting of slope transects measured in the field, a detailed geomorphological field map (1:2000) and existing contour lines with an interval of 20 m. Since the study area is fully covered with forest, this method was more time-efficient than using a tachymeter. In addition, the forest cover caused problems for photogrammetric height measurements using the available set of stereographic aerial photographs.

5.2. Tree distribution map

To obtain a tree distribution map, firstly, the regions of all the individual tree crowns in the study area were detected on the basis of the colour-infrared (CIR) orthophotos from 1996. In general, three different methods are described in the literature for detecting or delineating individual tree crowns from high spatial resolution aerial images (see Hill and Leckie, 1999). These are (1) detection of local intensity maximum (Blazquez, 1989; Dralle and Rudemo, 1996, 1997; Brandtberg and Walter, 1998; Uuttera et al., 1998; Wulder et al., 2000), (2) contour-based methods (Gougeon, 1995) and (3) template-based matching (Larsen and Rudemo, 1998). We firstly smoothed the orthophotos using a low pass filter. Subsequent segmentation of the image automatically delineated individual and clustered tree crowns. In addition, nonforested areas were segmented into homogenous areas. Segmentation was done in the software *eCognition* (Definiens-Imaging, 2003). Then, we used an object-based classification on the basis of membership functions related to local intensity maxima to classify all the segments in three classes, namely, tree crowns, clustered tree crowns and nontree crowns. This classification produced a tree crown map with an overall accuracy of 89.8% when compared with visually delineated tree crowns. We combined the obtained tree crown map with the forest inventory data to produce a tree distribution map, which represented the locations of trees and their DBH. The forest inventory provided data for 50 plots with a size of 30 × 50 m. These plots did not cover the whole test site that was used for the simulation modelling study. Therefore, the forest inventory data had to be extrapolated to obtain data for the remaining parts of the test site. For that, linear regression between the amount of raster cells classified as tree crowns in the tree crown map and the number of trees per hectare obtained from the forest inventory was used ($R^2 = 0.25$). The DBH of the trees covering the whole test site was uniformly randomly chosen between the minimum and maximum DBH that were measured in the forest inventory plots.

5.3. Rockfall simulation model

To simulate rocks that collide with tree stems, a computer model is needed that is able to calculate the motions of a falling rock realistically. Furthermore, such a simulation model should take different spatially distributed environmental characteristics into account, which influence the velocity and the direction of falling rocks. Therefore, we developed a model that combines a process-based and GIS-based model. The two main components of the model are the calculation of the falltrack of the rock and the calculation of the velocity of the falling rock. These calculations all started from predefined rockfall source areas.

Rockfall source areas were derived from the geomorphological field map. From each cell, defined as a rockfall source area, a single falling rock was simulated. The radius of this rock was 0.25 m, its initial velocity in horizontal direction (Vx) was 1 m/s and its initial velocity in vertical direction (Vy) was −1 m/s. The initial fall height in the cells that were used as rockfall start cells was set to 2 m. By doing this, we defined that the cliff faces from which rockfall start are at least 2 m high. With respect to the study area, this is a realistic value when using a grid with 2.5 × 2.5 m cells.

The mean slope gradient within each cell is derived from the DEM using the method described by Zevenbergen and Thorne (1987). Furthermore, the DEM was used for calculating the fall directions from each raster cell in the test site. For the latter, a modified multiple-flow algorithm (e.g. Quinn et al., 1991; Wolock and McCabe, 1995; Tarboton, 1997) is used, which is illustrated in Fig. 5. This method calculates the fall directions for the whole raster repeatedly for each simulation run by sampling the fall direction for each cell from a probability distribution, which is determined by the summed downslope gradient (SDG) from a central cell and the fraction of all the individual cells downslope of the central cell in the SDG. As a result, for each simulation run, falling rocks could be directed in different directions, which enables the simulation of diverging fall patterns.

The velocity of the falling rock is calculated with standard algorithms for a uniformly accelerated parabolic movement through the air and with algorithms modified from Pfeiffer and Bowen (1989) that calculate the energy balance before and after a collision (or bounce) on the slope surface. The modifications are that the factor compensating for the effect of the rockfall velocity on the elasticity of the collision is left out, since the empirical constants required for calculating this factor were not available for the study site. The model recalculates the velocity in x and y direction before a bounce into a tangential velocity (Vt_{in}), parallel to the slope surface following

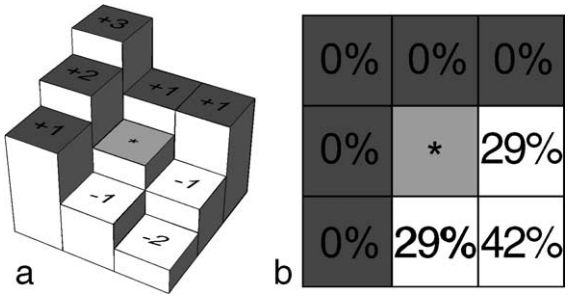

Fig. 5. (a) Example of a central cell (*) and its neighbouring cells and (b) the result of the calculation of the probabilities of the possible fall directions on the basis of the summed downslope gradient (SDG) for the example shown in (a).

$$Vt_{in} = Vy\sin(\beta) + Vx\cos(\beta) \quad (1)$$

and a normal velocity (Vn_{in}, perpendicular to the slope surface) following

$$Vn_{in} = Vy\cos(\beta) - Vx\sin(\beta) \quad (2)$$

where Vy = velocity in y direction (m/s); β = slope angle at the location of the bounce (°); and Vx = velocity in x direction (m/s). The tangential velocity after a bounce is then calculated with

$$Vt_{out} = \sqrt{\frac{(R^2(I\omega^2 + MVt_{in}^2))r_t}{(I + MR^2)}} \quad (3)$$

where Vt_{out} = tangential velocity after the bounce (m/s); R = radius of the falling rock (m); I = moment of inertia = $2/5{*}MR^2$ (kg m^2); ω = rotational velocity (1/s)=(Vt_{out} of the previous bounce)/R; M = mass of the falling rock (kg); Vt_{in} = tangential velocity before

the bounce (m/s); and r_t = tangential restitution coefficient determining energy loss (−), which is mainly determined by the vegetation cover and the roughness of the slope surface. The normal velocity after a bounce is calculated with

$$Vn_{out} = Vn_{in} r_n \quad (4)$$

where Vn_{out} = normal velocity after the bounce (m/s); Vn_{in} = normal velocity before the bounce (m/s); and r_n = normal restitution coefficient determining energy loss (−), which is mainly determined by the elasticity of the surface material covering the slope.

During each bounce, the slope angle at the exact location of the bounce is randomly decreased with an angle that varied between 0° and 4°. We programmed this to account for small-scale variability in the mean slope gradient, as shown in Fig. 6, which is 'smoothed-out' in the slope maps. This procedure is similar to the varying impact angle based on the surface roughness as described by Pfeiffer and Bowen (1989).

If the horizontal travelled distance of the rock between two simulated bounces is less than the diameter of the falling rock, the rock is considered to be rolling. In that case, the rock is given a new displacement over the slope surface equal to the diameter of the rock. This prevents an infinite amount of simulated bounces per raster cell (after Pfeiffer and Bowen, 1989). Sequences of motion through the air followed by a bounce are repeated until the velocity of the moving rock is equal to or less than 0.5 m/s.

Fig. 6. Photograph of the surface of a scree slope in the accumulation area of the test site, showing the small-scale variability in the mean slope gradient.

5.4. Coefficients of restitution

The slope characteristics that determine the elasticity of the surface material and thus the normal coefficient of restitution (r_n) are the composition of the material covering the surface and the vegetation cover. The slope characteristics that together determine the tangential coefficient of restitution (r_t) are the surface roughness, the vegetation cover (mainly trees and large shrubs) and the number of felled trees that are lying on the slope parallel to the contour lines that act as barriers. Another factor determining the tangential coefficient of restitution is the radius of the falling rock itself, since for larger rocks, the effective surface roughness is lower than for smaller rocks.

Standing trees affect the velocity of a falling rock as well because they act as barriers. Therefore, the model simulates collisions between falling rocks and standing trees. In case a collision occurs, this results in decrease of the kinetic energy and consequently a decrease of the velocity of the falling rock. The model is able to calculate whether these collisions occur, since the available tree distribution map defines the positions of the trees. Furthermore, the position of the falling rock is always known during simulation because the model simulated rocks as falling through the centre of the raster cells. If a collision between a rock and a tree occurs, the fraction of energy loss due to the collision is calculated on the basis of the position of the rock relative to the centre of the tree stem following

$$\Delta E = \sqrt{1 - \left(\frac{d}{0.5\mathrm{DBH} + R}\right)^2} \quad (5)$$

where ΔE = fraction of energy loss due to an impact against a tree stem (−); d = distance between the centre of the rock and the centre of the tree stem (m); DBH = diameter of the tree stem at breast height (m); and R = radius of the falling rock (m). We developed this formula assuming that a tree stem absorbs a maximum amount of kinetic energy if a

central collision between a rock and a tree stem occurs. We did not make any distinctions between the energy absorbed by different tree species because of lack of data.

In reality, falling rocks could collide with trees at a certain height above the surface. Subsequently, a rock falls on the ground and gains new kinetic energy. This process is incorporated in the model by limiting the maximum energy loss to 99%. After the energy loss is calculated, the translation and rotation energy is multiplied by the calculated fraction of energy loss. Next, the resulting energies are transformed into a resultant velocity. If a falling rock does not collide with a tree stem, energy is lost because of a bounce on the slope surface. The amount of energy loss is then defined by r_n and r_t. To analyse the effect of these parameters on the velocity before and after a bounce, a single bounce was repeatedly simulated. During these simulations, one single parameter was varied, while the other parameters involved were given a constant value. This was done for the r_n, the r_t, the radius of the rock and the mass of the rock.

The outcomes of this test showed mainly that the r_t and the radius of the rock affect the energy loss during a bounce (Fig. 7). Since the bounce is the most important part of the model that determines the energy loss, the r_t and the radius of the rock are the main parameters determining energy loss in the model. The radius of the simulated falling rocks was constant for all the model simulations ($R = 0.25$ m); therefore, the r_t is the most important parameter determining the deceleration of the simulated falling rocks. The slope gradient is the most important parameter determining the acceleration. The findings mentioned above justified the choice to estimate the r_n on the basis of the mapped slope characteristics in combination with literature data (Pfeiffer and Bowen, 1989; van Dijke and van Westen, 1990; Kobayashi et al., 1990; Giani, 1992; Azzoni et al., 1995; Chau et al., 1998, 2002; Meißl, 1998). The r_t varied between estimated minimum and maximum values, which were consistent with literature data. The actual values of r_t, however, were determined by the slope characteristics that were measured and

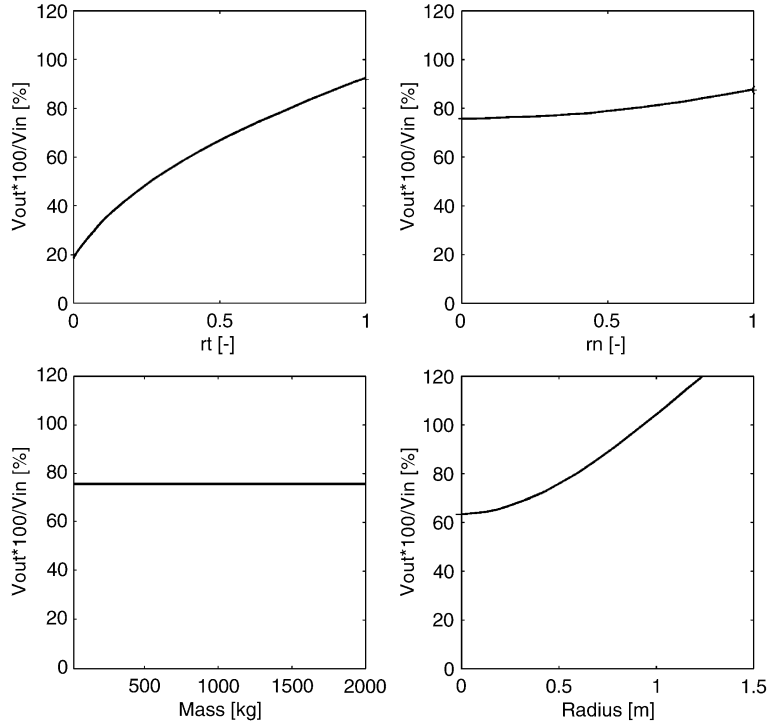

Fig. 7. The effect of the r_t, the r_n, the mass and the radius of the rock on the change of the velocity before and after a single bounce.

estimated in the field. To determine the tangential coefficient of restitution (r_t), the following formula was developed

$$r_t = \max - (\text{range}*\text{fraction}) \quad (6)$$

where max = maximum r_t value (–) = 0.95; range = range of r_t values (–) = max – min; min = minimum r_t value (–) = 0.01; and fraction = the fraction of the r_t that is attributed to the mapped slope characteristics (–). This was calculated with the following formula:

$$\text{fraction} = (SC_1 wSC_1 + SC_2 wSC_2 + \ldots + SC_i wSC_i) / (wSC_1 + wSC_2 + \ldots + wSC_i) \quad (7)$$

where SC_i = slope characteristic i and wSC_i = weight of the slope characteristic i. As shown in Table 3, different weights were addressed to each different slope characteristic. Only the extreme weight settings were tested to evaluate the effect of changing proportions of the mapped slope characteristics. One hundred simulation runs were carried out for evaluating a weight setting according to the *Monte Carlo* method (Lewis and Orav, 1989). For each simulation run, a new fall direction map was calculated using the previously mentioned modified multiple-flow algorithm. The mass and the radius of the rock and the locations of the rockfall source cells were similar for all the executed simulations. A generalised diagram of all the described model steps is presented in Fig. 8.

5.5. Validation

Data for validating the model results were both provided by the detailed forest inventory data and the geomorphological field map. Within the area covered by the forest inventory, 18 squares of 25 × 25 m were randomly selected, which were all situated within a single forest inventory grid cell. For these 18 squares, the tree volume per hectare and the number of scars per hectare caused by rock impacts were measured. These data were compared with the number of rock impacts on trees as simulated by the model. For standardisation purposes, both the validation data (observed values) and the simulated data (predicted values) within the 18 squares were expressed as percentages of the summed values within all the randomly selected squares. In detail, the observed value represented the number of scars per tree volume unit in a square expressed as percentage of the total number of scars per tree volume unit in all squares. Here, the number of scars per tree volume unit was the number of scars per hectare caused by rock impacts divided by the tree volume within the square. The predicted value represented the number of impacts in a square expressed as percentage of the summed number of impacts in all squares. For all the model

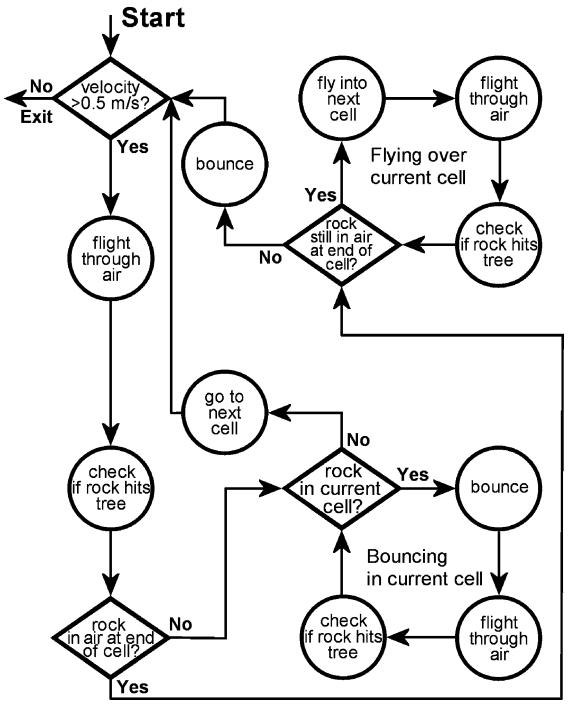

Fig. 8. Flow diagram showing the simulation of a single rock falling from a start in the developed rockfall model.

Table 3
Weight settings for the slope characteristics determining the tangential coefficient of restitution (r_t), which provided the best results

Slope characteristic	Weight	Weight range
Wooden barriers/felled trees	10	1–10
Surface roughness 1 m	3	1–10
Surface roughness 5 m	3	1–10
Surface roughness 20 m	3	1–10
Rockfall resistant shrubs	1	1–10

Table 4
Results produced by the model with optimal weight settings for the r_t as shown in Table 3

Validation data	ME	MSE	R^2
Damaged trees	0.0	0.24	–
Mapped recent rock accumulations	–	–	0.74

outcomes, the mean error (ME) and the mean squared error (MSE) were calculated following

$$\mathrm{ME} = \frac{1}{n}\sum_{i=1}^{n}(P_i - O_i) \quad (8)$$

$$\mathrm{MSE} = \frac{1}{n}\sum_{i=1}^{n}(P_i - O_i)^2 \quad (9)$$

where n is the number of observations, P_i is the modelled or predicted value in raster cell i and O_i is the observed value in raster cell i.

In addition to the size distribution of rocks throughout the test site, the geomorphological map also included the locations of recent scree and rock accumulation areas throughout the test site. This could be determined first by the absence of mosses and vegetation covering the accumulated material and second by the relative age of the deposits as inferred from the slope morphology. Within all the validation squares described in the previous paragraph, it is evaluated whether a cell modelled as an end location of a falling rock was also mapped as a recent accumulation area. This provides a Boolean dataset with a modelled and a mapped value (rockfall accumulation: value = 1, if not: value = 0) for every cell within all validation squares. On the basis of this dataset, the R^2 is calculated.

6. Simulation model results

The developed model produced rockfall runout zones that ranged from the source areas to the upper half of the accumulation area. This pattern was identical for each tested weight setting for the slope

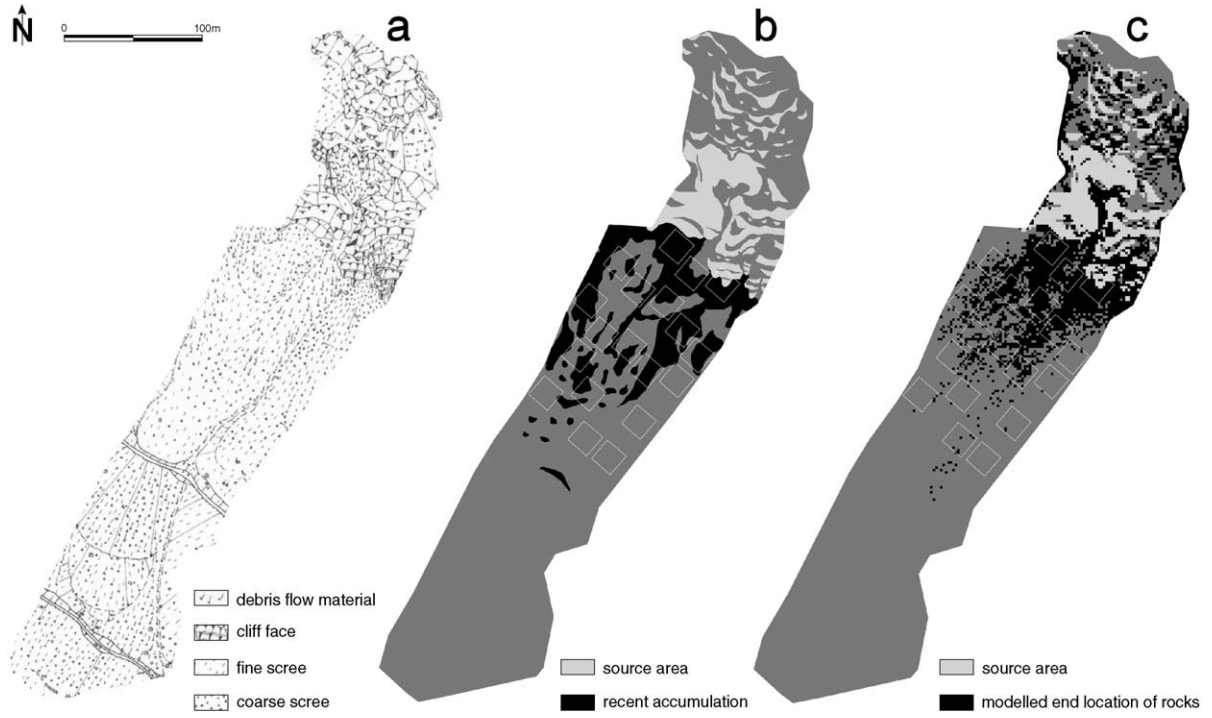

Fig. 9. (a) The geomorphological map of the test site. (b) Map showing the active or recent accumulation areas, as derived from the geomorphological map and field observations. (c) Map showing the simulated end locations or accumulation areas after 100 simulation runs using the optimal settings and a rock radius of 0.25 m. The white outlined squares are the validation squares.

characteristics determining r_t. During fieldwork, it was observed that most of the falling rocks stop within the upper part of the accumulation area. Only some rocks fall down the transport channel and reach the upper forest road. The developed model confirms this as the number of rocks reaching the upper forest road was less than 5% of the total number of falling rocks in all the simulations. In that sense, all the simulations produced comparable results. Changing the weight setting for the slope characteristics determining the r_t did, however, result in significant variation in the extent and location of local accumulation areas throughout the upper half of the accumulation area. Validation of the model results with the data on damaged trees and mapped recent rock accumulations showed that the best results were produced if the settings shown in Table 3 were used. This resulted in an R^2 of 0.74 for the correlation between the mapped and modelled accumulation areas, and this setting produced the lowest mean squared error (MSE = 0.24) between the spatial distribution of modelled impacts and the spatial distribution of the number of scars on tree stems (Table 4).

The optimal weight settings shown in Table 3 assign a high importance to the number of wooden barriers in a homogeneous terrain unit. Within this setting, wooden barriers are more than three times more important than the surface roughness measured on the 1-, 5- and 20-m transects. Different weights for these three surface roughness values were also tested, but optimal results are produced if their weights are equivalent. These results also indicate that rockfall resistant shrubs are least important for decelerating falling rocks.

Fig. 9 shows the field mapped geomorphological map of the test site (Fig. 9a), the derived recent scree accumulation map (Fig. 9b) and the result of the simulation during which the optimal weight settings were used (Fig. 9c). A black coloured cell shown in Fig. 9c indicates that, at least during one simulation, a rock stopped within that cell. Thus, it is also possible that a larger number of rocks stopped in that cell. This map only visualises the accumulation patterns, whereas the frequency map (not presented here) showed that most rocks stopped in the upper part of the accumulation area, where the dense black cloud is visible in Fig. 9c. Thus, only a few simulated rocks

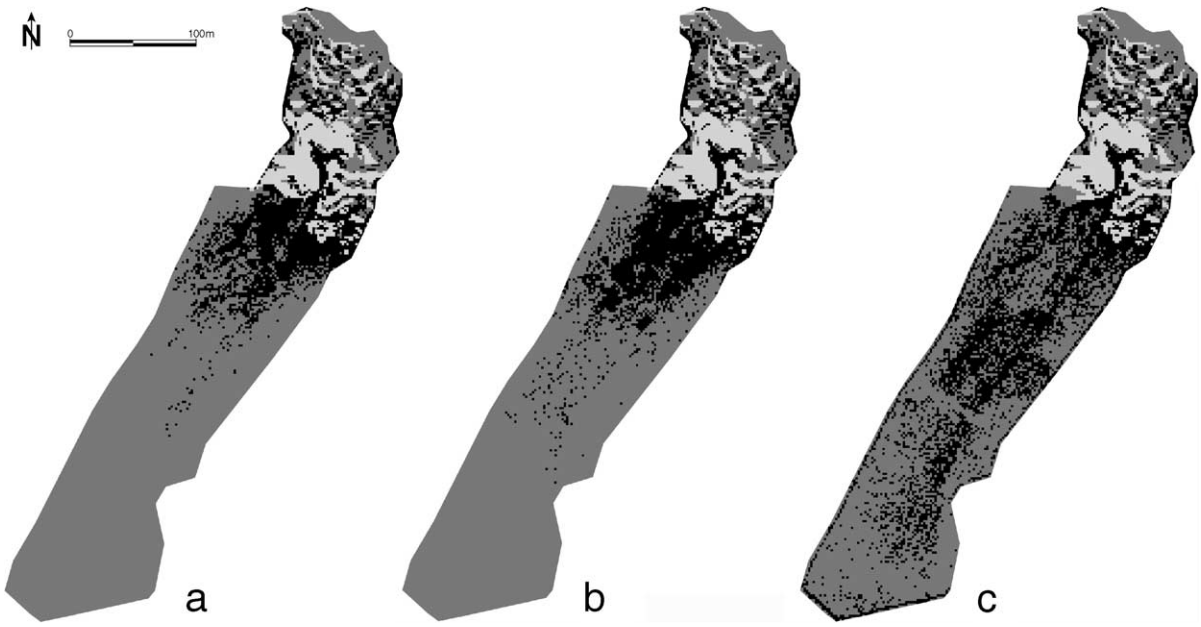

Fig. 10. (a) Map showing the simulated end locations or accumulation areas using the optimal settings, a rock radius of 0.25 m and the current forest cover; (b) idem., only with 50% less tree density; (c) same simulation, only without forest cover. All the graphs are the result of 100 simulation runs.

reached the upper forest road, which is shown in the geomorphological map (Fig. 9a).

To analyse the change of the rockfall hazard if the protection forest continues to deteriorate, the simulation model, which seemed to predict current accumulation patterns satisfactorily, was used to test scenarios with a random tree distribution with 50% fewer trees (case B) and with no trees covering the site at all (case C). The results of these simulations show that the amount of rocks reaching the valley is still zero in case B (Fig. 10b). A distinct difference is that more rocks reach the upper forest road. In case C, however, many rocks reached the lower boundary of the test site (Fig. 10c). There, the velocities of the rocks were still approximately 20 m/s.

7. Discussion

The protection forest that covers the study area is almost continuously under attack by rockfall, but especially during the spring and after heavy rain. Therefore, we consider water infiltrating in joints and frost shattering as the main trigger for rockfall in the study area. The primary cause, however, that rockfall source areas occur in the study area is because of the effect of glaciations during the Pleistocene glacial periods. Glacial erosion of competent geological formations resulted in oversteepened slopes. Postglacial relaxation of these slopes led to the development of tensional fissures and rock creep, which causes additional destabilisation of the original slopes. The steep slope gradient in combination with the unfavourable dips and dip directions of the major joint sets and the bedding planes in the study area leads to breaking out of mainly relatively small rocks (largest diameter between 0.25 and 0.5 m). Rocks in the bottom parts of the cliff face break out first; subsequently, this process slowly migrates up along the cliff face. This preferentially occurs in relation to the tensional fissures along the steep valley slopes.

At the intersection of the cliff face and the largest fissures, three major denudation niches have developed. From these niches, large amounts of detached material have been removed, deposited and consequently forming large talus slopes. In the lower zone, below the lower forest road, many fossil rock accumulations were found. This suggests that these accumulations were largely built up during a nonforested period. In the Alps, the Late Glacial or even the Early Holocene is known for its intense frost shattering, lack of forests and unstable (rock) slopes (Flint, 1971; De Graaff et al., 1989). The rock material probably moved downslope as rock avalanches, debris flows and rockfall.

The accumulation area below the denudation niches consists of large identifiable talus cones that gradually fuse into one another down the accumulation slope. At present, the rockfall activity within the denudation niches is comparable to the other steep cliff faces on the nondissected mountain face between the large denudation niches. The latter currently produce rocks that fall down and fill up local depressions between the larger talus cones in the upper part of the study area. Rocks originating from the large denudation niches fall down the slope into the forest and stop in local accumulation areas where the surface roughness is high because of previously deposited large rocks. Another observed feature is that rocks accumulate behind standing trees or felled trees that lie diagonally or perpendicular to the slope direction. Small rocks are deposited in the upper part of the accumulation area or even in the transport channel of the niches. Occasionally, rocks originating from the niches fall all the way down the existing transport channels, which have been denuded of trees by both snow avalanches and rockfalls, underneath the denudation niches.

Our simulation model, which was developed using the obtained field knowledge, confirmed the abovementioned observations for the modelling test site. This model showed that, in decreasing order of importance, firstly, standing and felled trees, secondly, the surface roughness and, thirdly, the rockfall resistant shrubs are the determining factors for the distribution of rockfall-affected areas in our test site. As mentioned before, only a relatively small number of rocks fall through the transport channel, but rocks that do so gain a high velocity because the surface roughness in the channel is low and trees or shrubs are absent. The latter is due to the fact that falling rocks destroy seedlings. In addition, snow creep and snow avalanches starting in the denudation niches also contribute to restriction of growth or even removal of seedlings. An increased tree density, both in the transport channel and in the source area, could reduce

the impact of all these disturbing processes. In short, the degradation of the protection forest in the area underneath the denudation niches is a self-reinforcing process, which needs to be reversed.

Both the simulation results and field observations showed that many falling rocks stop within the upper-forested part of the accumulation area. Though, a point of attention is the lack of regeneration of the forest, which is needed to provide backup and ensure protection in the future. If this situation does not improve and the forest continues to break down, a similar self-reinforcing process is to be expected in the whole study area as in the earlier-mentioned transport channels underneath the denudation niches. We simulated these situations by using, firstly, 50% of the current forest density and, secondly, by simulating no forest cover at all. The results showed that a reduction of the tree density by 50% increases the rockfall hazard to some extent, but an absence of the forest cover resulted in rocks reaching the main valley and thus significantly increased the rockfall hazard. Again, to prevent this situation, the primary forest management goals in the area should be to increase the regeneration and to create opportunities for trees to cover the transport channel. To achieve the latter, temporary protective measures against rockfall have to be taken in the denudation niches such as the construction of wooden barriers by placing felled trees slightly diagonal to the slope direction. By doing this, the velocity of falling rocks will be reduced, but transport will continue in a more controlled manner. This prevents accumulation of rock material on the slope, in contrast to most technical rockfall protection constructions. Another advantage is that the decaying felled trees provide excellent seedbeds for seedlings, which could stimulate regeneration. Promotion of regeneration is the second important forest management goal in the area. Hunting management has a large responsibility in this as well because this can protect seedlings against excessive browsing.

The model developed in this study simulated rockfall for a static, given situation both regarding the state of the forest and the slope characteristics. Progress could be made by coupling rockfall simulation and forest growth in a dynamic model. Such a model would be more suitable to test forest management interventions and its effect on the future protective function of the forest. The dynamic rockfall model should incorporate changes of surface characteristics due to deposition of material, like an increase in the surface roughness. Furthermore, the same model could calculate damages on trees. This could be taken into account in the dynamic forest growth model in which regeneration, growth and breakdown are simulated. This would change the initial tree distribution and therefore indirectly the distribution of active rockfall tracks. To simulate tree damages caused by rockfall impacts more accurately, a better characterisation of the mechanical behaviour of a tree after a rock impact is needed in the developed model. The experimental data required for this characterisation are currently lacking and need to be investigated.

Regarding the coefficients of restitution in our model, stochastic simulation enables us to model realistic value ranges. An example is the Monte Carlo simulation, where minimum and maximum values of the coefficients of restitution are determined by the outcome of a dynamic coupled forest growth–rockfall model, in which the spatial covariance between the surface roughness and the distribution of both standing and lying trees is represented.

8. Conclusions

The slope gradient, the various geological formations and their geotechnical properties of the bedrock are the main controlling factor for rockfall in the study area. The potential rockfall source areas were mapped at 1:2000 and used in the developed rockfall simulation model. The results showed that the current accumulation patterns throughout the study area could be modelled accurately. On the basis of a developed formula for estimating the tangential coefficient of restitution and the model tests, we conclude that, in decreasing order of importance, standing and felled lying trees, the surface roughness and rockfall resistant shrubs primarily determine the distribution of rockfall-affected areas in the test site used for simulation modelling within the study area. Deposits of older events such as rock avalanches, debris flows as well as rockfall were identified and mapped in the lowest parts of the accumulation area. Model simulation of the current field situation produced considerable shorter rockfall runout zones due to the protective function of the forest. The simulation test

without a forest cover produced rockfall similar run-out zones as the older rockfall events. The tests showed that these events occurred under different conditions than the current ones. We assume that the lowest deposits in the accumulation area are related to events that occurred in the Late Glacial or Early Holocene. Finally, we believe that a combined field research and modelling approach as applied in this study is a prerequisite for better understanding the dynamics of rockfall on a forested slope. For a better understanding of the feedbacks between rockfall and forest growth, for example, to predict the long-term effects of forest management interventions, we recommend the development of a dynamic rockfall–forest growth model.

Acknowledgements

We gratefully thank Sanneke van Asselen, Monique Blankers and Christopher Dich for their contributions to this work. Furthermore, we thank the Research Foundation for Alpine and Subalpine Environments (RFASE) and Stand Montafon Forstfonds for supporting this research.

References

Ammer, C., 1996. Impacts of ungulates on structure and dynamics of natural regeneration of mixed mountain forests in the Bavarian Alps. Forest Ecology and Management 88, 43–53.

Azzoni, A., Barbera, G.L., Zaninetti, A., 1995. Analysis and prediction of rockfalls using a mathematical model. International Journal of Rock Mechanics and Mining Science 32, 709–724.

Bitterlich, W., 1948. Die Winkelzählprobe. Allgemeine Forst- und Holzwirtschaftliche Zeitung 1, 4–5.

Blazquez, C.H., 1989. Computer-based image analysis and tree counting with aerial color infrared photography. Journal of Imaging Technology 15 (4), 163–168.

Bozzolo, D., Pamini, R., 1986. Simulation of rock falls down a valley side. Acta Mechanica 63, 113–130.

Brandtberg, T., Walter, F., 1998. Automated delineation of individual tree crowns in high spatial resolution aerial images by multiple-scale analysis. Machine Vision and Applications 11, 64–73.

Budetta, P., Santo, A., 1994. Morphostructural evolution and related kinematics of rockfalls in Campania (southern Italy): a case study. Engineering Geology 36, 197–210.

Bull, W.B., King, J., Kong, F.C., Moutoux, T., Phillips, W.M., 1994. Lichen dating of coseismic landslide hazards in alpine mountains. Geomorphology 10, 253–264.

Carson, M.A., Kirkby, M.J., 1972. Hillslope Form and Process. Cambridge Univ. Press, Cambridge. 475 pp.

Chau, K.T., Wong, R.H.C., Lee, C.F., 1998. Rockfall problems in Hong Kong and some new experimental results for coefficient of restitution. International Journal of Rock Mechanics and Mining Science 35, 662–663.

Chau, K.T., Wong, R.H.C., Wu, J.J., 2002. Coefficient of restitution and rotational motions of rockfall impacts. International Journal of Rock Mechanics and Mining Science 39, 69–77.

Definiens-Imaging, 2003. eCognition, object oriented image analysis. http://www.definiens-imaging.com/.

De Graaff, L.W.S., Jong, M.G.G.D., Rupke, J., Verhofstad, J., 1987. A geomorphological mapping system at scale 1:10,000 for mountainous areas. Zeitschrift für Geomorphologie N.F. 31, 229–242.

De Graaff, L.W.S., Kuijper, W.J., Slotboom, R.T., 1989. Die Schlussvereisung und die spätglaziale Entwicklung des Moorgebietes Gasserplatz, Feldkirch-Göfis, Vorarlberg. Jahresbericht-Geologische Bundesanstalt 132, 197–413.

Dralle, K., Rudemo, M., 1996. Stem number estimation by kernel smoothing of aerial photos. Canadian Journal of Forest Research 26, 1228–1236.

Dralle, K., Rudemo, M., 1997. Automatic estimation of individual tree positions from aerial photos. Canadian Journal of Forest Research 27, 1728–1736.

ESRI, 2003. Arcinfo. http://www.esri.com/software/arcgis/arcinfo/index.html.

Evans, S.G., Hungr, O., 1993. The assessment of rockfall hazard at the base of talus slopes. Canadian Geotechnical Journal 30, 620–636.

Flint, R.F., 1971. Glacial and Quaternary Geology. Wiley, New York.

Giani, G.P., 1992. Rock Slope Stability Analysis. Balkema, Rotterdam. 361 pp.

Gougeon, F.A., 1995. Comparison of possible classification schemes for tree crowns individually delineated on high spatial resolution MEIS images. Canadian Journal of Forest Research 21, 1–9.

Hétu, B., Gray, J.T., 2000. Effects of environmental change on scree slope development throughout the postglacial period in the Chic-Choc Mountains in the northern Gaspé Peninsula, Québec. Geomorphology 32, 335–355.

Hill, D.A., Leckie, D.G., 1999. Automated interpretation of high spatial resolution digital imagery for forestry. Proceedings International Forum, 10–12 February 1998. Natural Resources Canada, Canadian Forest Service, Victoria, British Columbia, Canada. 402 pp.

Hocking, G., 1976. A method for distinguishing between single and double plane sliding of tetrahedral wedges. International Journal of Rock Mechanics and Mining Science 13, 225–226.

Hoek, E., Bray, J.W., 1981. Rock Slope Engineering. Institution of Mining and Metallurgy, London, UK. 358 pp.

Hoek, E., Brown, E.T., 1997. Practical estimates of rock mass strength. International Journal of Rock Mechanics and Mining Science 34, 1165–1186.

Jahn, J., 1988. Entwaldung und Steinschlag. Proceedings of the International Symposium, Interpraevent, July 1988, Graz. Tagungspubl. Bd. vol. 1, pp. 185–198.

Jomelli, V., Francou, B., 2000. Comparing the characteristics of

rockfall talus and snow avalanche landforms in an Alpine environment using a new methodological approach: Massif des Ecrins, French Alps. Geomorphology 35, 181–192.

Kirkby, M.J., Statham, I., 1975. Surface stone movement and scree formation. Journal of Geology 83, 349–362.

Kobayashi, Y., Harp, E.L., Kagawa, T., 1990. Simulation of rockfalls triggered by earthquakes. Rock Mechanics and Rock Engineering 23, 1–20.

Larsen, M., Rudemo, M., 1998. Optimizing templates for finding trees in aerial photographs. Pattern Recognition Letters 19, 1153–1162.

Lewis, P.A.W., Orav, E.J., 1989. Simulation Methodology for Statisticians, Operations Analysts, and Engineers, vol. 1. Wadsworth and Brooks/Cole, Pacific Grove.

Markland, J.T., 1972. A useful technique for estimating the stability of rock slopes when the rigid wedge sliding type of failure is expected. Imperial College Rock Mechanics Research Report No. 19.

Meißl, G., 1998. Modellierung der Reichweite von Felsstürzen. Fallbeispeile zur GIS-gestützten Gefahren-beurteilung aus dem Beierischen und Tiroler Alpenraum. PhD Thesis, Universität Innsbruck, Innsbruck. 249 pp.

Motta, R., 1996. Impact of wild ungulates on forest regeneration and tree composition of mountain forests in the Western Italian Alps. Forest Ecology and Management 88, 93–98.

Motta, R., Haudemand, J.C., 2000. Protective forests and silvicultural stability—an example of planning in the Aosta Valley. Mountain Research and Development 20, 180–187.

Okura, Y., Kitahara, H., Sammori, T., Kawanami, A., 2000a. The effects of rockfall volume on runout distance. Engineering Geology 58, 109–124.

Okura, Y., Kitahara, H., Sammori, T., 2000b. Fluidization in dry landslides. Engineering Geology 56, 347–360.

Pfeiffer, T.J., Bowen, T.D., 1989. Computer simulation of rockfalls. Bulletin of the Association of Engineering Geologists XXVI, 135–146.

Quinn, P., Beven, K., Chevallier, P., Planchon, O., 1991. The prediction of hillslope flow paths for distributed hydrological modelling using digital terrain models. Hydrological Processes 5, 59–79.

Seijmonsbergen, A.C., 1992. Geomorphological evolution of an alpine area and its application to geotechnical and natural hazard appraisal in the NW. Rätikon and S. Walgau (Vorarlberg, Austria), including map series at 1:10,000 scale. PhD Thesis, University of Amsterdam, Amsterdam. 109 pp.

Shiver, B.D., Borders, B.E., 1995. Sampling Techniques for Forest Resource Inventory. Wiley, New York. 356 pp.

Statham, I., 1976. A scree slope rockfall model. Earth Surface Processes 1, 43–62.

Statham, I., Francis, S.C., 1986. Influence of scree accumulation and weathering on the development of steep mountain slopes. In: Abrahams, A.D. (Ed.), Hillslope Processes. Allen and Unwin, Winchester, pp. 245–267.

Tarboton, D.G., 1997. A new method for the determination of flow directions and upslope areas in grid digital elevation models. Water Resources Research 33, 309–319.

van Dijke, J.J., van Westen, C.J., 1990. Rockfall hazard, a geomorphological application of neighbourhood analysis with ILWIS. ITC Journal 1, 40–44.

Uuttera, J., Haara, A., Tokola, T., Maltamo, M., 1998. Determination of the spatial distribution of trees from digital aerial photographs. Forest Ecology and Management 110, 275–282.

Wieczorek, G.F., Jäger, S., 1996. Triggering mechanisms and depositional rates of postglacial slope-movement processes in the Yosemite Valley, California. Geomorphology 15, 17–31.

Wieczorek, G.F., Snyder, J.B., Waitt, R.B., Morrissey, M.M., Uhrhammer, R.A., Harp, E.L., Norris, R.D., Bursik, M.I., Finewood, L.G., 2000. Unusual July 10, 1996, rock fall at Happy Isles, Yosemite National Park, California. Geological Society of America Bulletin 112, 75–85.

Wolock, D.M., McCabe Jr., G.J., 1995. Comparison of single and multiple flow direction algorithms for computing topographic parameters in TOPMODEL. Water Resources Research 31, 1315–1324.

Wulder, M., Niemann, K.O., Goodenough, D.G., 2000. Local maximum filtering for the extraction of tree locations and basal area from high spatial resolution imagery. Remote Sensing of Environment 73, 103–114.

Zevenbergen, L.W., Thorne, C.R., 1987. Quantitative analysis of land surface topography. Earth Surface Processes and Landforms 12, 47–56.

Zvelebil, J., Moser, M., 2001. Monitoring based time-prediction of rock falls: three case-histories. Physics and Chemistry of the Earth (B) 26 (2), 159–167.